Central European Journal of Energetic Materials
ISSN 1733-7178; e-ISSN 2353-1843

Cent. Eur. J. Energ. Mater. 2024, *21*(1): 80-107; DOI 10.22211/cejem/186565
Article is available in PDF-format, in colour, at:
https://ipo.lukasiewicz.gov.pl/wydawnictwa/cejem-woluminy/vol-21-nr-1/

Research paper

Initiation Strategy of Aimable Warhead Based on Asynchronous Initiation between Lines

Shukai Zhang[1,2)], **Xiaowei Ren**[3)], **Qing Guo**[1)], **Xiaogang Li**[1)], **Haoyu Zhang**[1)], **Yuquan Wen**[1,*)]

[1)] *State Key Laboratory of Explosion Science and Technology, Beijing Institute of Technology, China*

[2)] *Shandong Institute of Non-metal Materials, China*

[3)] *China Airborne Missile Academy, China*

* *E-mail:* wyquan@bit.edu.cn

Abstract: Asymmetrically initiated (AI) warhead has been widely used to strike air targets. To improve the accuracy and power of AI warhead, asynchronous initiation between lines was proposed. The power and dispersion characteristics of prefabricated fragments under different initiation schemes were studied by LS-DYNA simulation. The results show that asynchronous initiation between lines can regulate fragment velocity and its distribution by changing the trajectory and action position of the high-pressure area. The results of preferred strategies under sextile asynchronous initiation are similar to or even better than that of simultaneous initiation under 12 quantiles. The accuracy can be improved from 30° to 15° by setting a single delay of 1.109 μs under sextile initiation. Compared with the single point initiation, the gain of the maximum initial velocity is 19.0-25.3% under the asynchronous initiation strategy between lines. The maximum deviation of fragments orientation azimuth and flight direction are both 1.4°.

Keywords: aimable warhead, asynchronous initiation, orientation accuracy, power characteristics, initiation strategy

Supplementary Information (SI):
SI contains a datasheet in Excel with results for two-line initiation

1 Introduction

Precision strikes and efficient damage have become essential trends for missiles with the increasing mobility and protection of air targets [1, 2]. Asymmetrically initiated (AI) warheads have been widely used because of their simple structure and mature technology [3]. The fragment velocity in the aim direction can be increased by 20-30% compared with the same warhead initiated along the central axis by initiating the initiation lines opposite the target. However, the power and accuracy of AI warheads are still limited. The Target Detection Device (TDD) can accurately obtain the miss direction of the target at present [4] For example, the target azimuth recognition error of laser fuze based on quadrant subdivision is no more than 15° [5]. However, the angular resolution of the aimable direction is generally only 22.5-45° because of the limitation of the initiation quantiles [4]. Meanwhile, the number of high-speed fragments is limited due to the limited size of the Mach overpressure area [6]. When the miss distance is large or the target is small, it is difficult to realize an aimable strike truly if the high-speed fragments fail to hit the target due to poor orientation accuracy. Therefore, improving the orientation accuracy of high-speed fragments is a pressing problem.

One solution is to increase the number of high-speed fragments. The wide strike range can make up for the lack of orientation accuracy and increase the damage probability. Xu *et al.* [7] designed a hollow cylindrical regulator with evenly distributed grooves which can realize the collision and superposition of circumferential multi-waves by single detonator initiation at the end face. The number of Mach rods can be controlled by the number of grooves. However, the regulator will reduce the charge and increase the difficulty of the charging process. In addition, the warhead with an asymmetric shell can also increase the number of fragments in a specific direction. D-shape casing is a common and basic type of asymmetric shell, which is usually used in rotating aimable warhead and deformable warhead [8]. Directional fragment generator warhead can also project more fragments in a coherent conical beam toward the target, because its fragments are located on the end face of charge [9]. However, it takes time to complete the deformation or rotation, which may result in missing the best initiation time because the intersection process of missile and target is transient.

Another solution is to adjust the initiation mode. The scattering direction of fragments can be controlled by multi-point initiation. Most of these studies have mainly focused on eccentric simultaneous initiation [10-13]. Under simultaneous initiation, increasing the initiation quantile can refine the resolution of the orientation angle. However, the fragment velocity will decrease if the number of quantiles continues to increase when the included angle of initiation quantiles

is smaller than a certain value [11, 12]. In recent years, asynchronous initiation in-line has become an important strategy to control the axial dispersion angle of fragments [14, 15]. Liu *et al.* [16] studied the influence of initiation delay on velocity and axial direction angle of fragments under sequential initiation. Zhang *et al.* [17] compared the damage efficiency of blast-fragmentation warheads under sequential initiation and simultaneous initiation. Asynchronous initiation can change the position and direction of overpressure area and control the dispersion of fragments. It is expected to achieve adjustable orientation and power gain by setting the initiation delay between lines. However, there are few reports aiming to investigate asynchronous initiation between lines.

This work proposes a method to improve the directional accuracy and power of aimable warhead based on asynchronous initiation between lines. A calculation model of the trajectory of the high-pressure area caused by detonation wave collision under asynchronous initiation is given. A full-scale numerical model simulating the action process of warhead is established and verified by experimental data. The influence of time delay on directional ability and power characteristics is studied. The best initiation strategy is given when the target is in different miss directions, which will provide a technical way to improve the directional accuracy and strike power of aimable warhead.

2 Computational Model

2.1 Trajectory of the high-pressure area

2.1.1 Mathematical model

A model of the charge section shown in Figure 1 is established to investigate the trajectory of the high-pressure area generated by the detonation wave collision under asynchronous initiation between lines. Because the initiations in the same line are simultaneous and the rarefaction waves from the ends are ignored, the warhead model could be simplified as two-dimensional [3]. The radius of the charge is R, and the origin of the coordinate system coincides with the circle center. I_1 and I_2 are two initiation points representing the initiation lines in the 3D structure. I_1 detonates first, then I_2 detonates after Δt. To simplify the problem, the shape of the high-pressure area is ignored. From t to t', the high-pressure area moves from A to B.

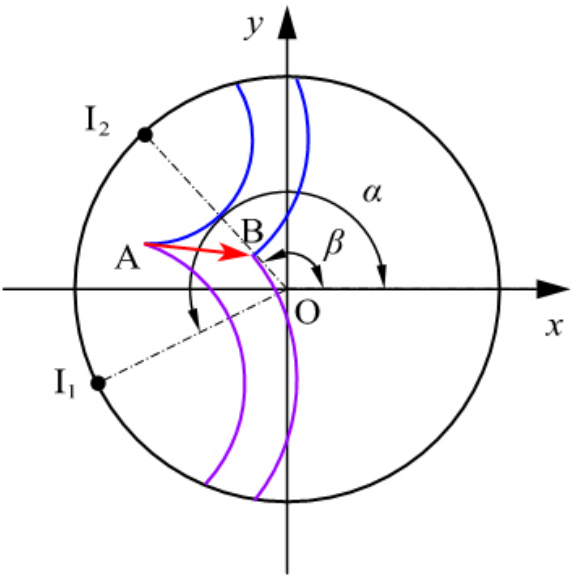

Figure 1. Trajectory of the high-pressure area

The model is based on the assumptions of uniform charge and the nonexistence of detonation growth. The propagation of detonation wave follows the principle of geometric optics [18]. Solving the trajectory of the high-pressure area caused by the collision of two detonation waves with fixed initiation delay is equivalent to solving the intersection of a series of circles with a constant radius difference [19]. The equations of the two shock wave circles at time t are as follows when the timing starts after I_2 initiates.

$$\begin{cases} \left(x - R\cos\alpha\right)^2 + \left(y - R\sin\alpha\right)^2 = \left[\left(\Delta t + t\right)D\right]^2 \\ \left(x - R\cos\beta\right)^2 + \left(y - R\sin\beta\right)^2 = \left(tD\right)^2 \end{cases} \tag{1}$$

where D is the detonation velocity of the charge, α or β is the angle from the intersection of the warhead circle and the positive x-axis to the initiation point by rotating counterclockwise around the center. Equation 1 should satisfy $0 \le \Delta t < \Delta t_{max}$ and $t \ge t_{min}$. The expression of maximum delay Δt_{max} and initial time t_{min} of detonation wave collision are following.

$$\Delta t_{\max} = \frac{\sqrt{2}R}{D}\sqrt{1-\cos(\alpha-\beta)} \tag{2}$$

$$t_{\min} = \frac{\sqrt{2}R\sqrt{1-\cos(\alpha-\beta)} - D\Delta t}{2D} \tag{3}$$

2.1.2 Model validation

A two-dimensional model simulating the asynchronous initiation between lines is established in LS-DYNA to verify our model, where $\alpha = 210°$, $\beta = 150°$, $R = 65.5$ mm, $D = 7980$ m/s. Figure 2 shows the comparison of the calculation and the simulation of the trajectory under the delay of 0, 2 and 4 μs. The calculation shows a good agreement with the simulated results. Equation 1 can predict the trajectory of the high-pressure area and can be used to guide the design of initiation schemes.

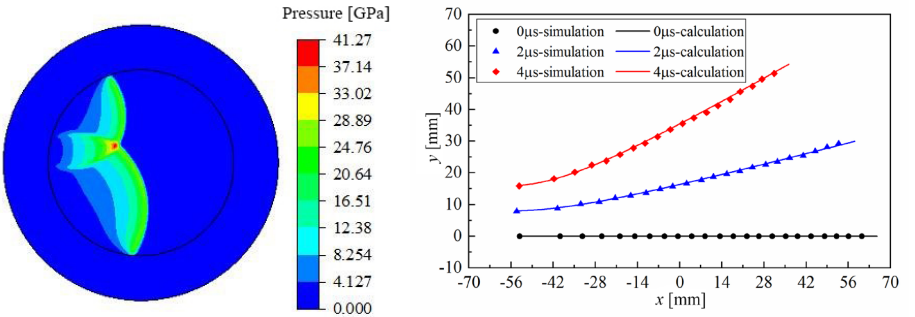

(a) (b)

Figure 2. Pressure cloud map (a) and comparison of trajectories (b) of the high-pressure area

2.2 Numerical simulation of aimable warhead

2.2.1 Finite Element Model

Figure 3 shows the finite element model established in TrueGrid. Air and shell are hidden for illustrating the warhead structure. The length of the warhead is 295 mm, and the diameter is 155 mm. The charge is Comp. B with a diameter of 131 mm. Spherical prefabricated fragments with a diameter of 6 mm are staggered between the shell and the liner.

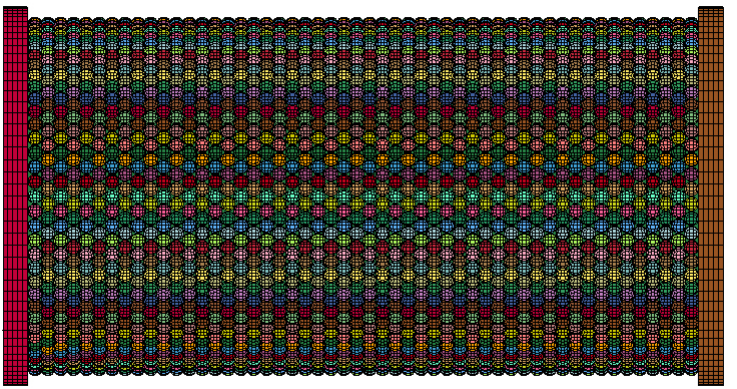

Figure 3. Finite element model of warhead

LS DYNA is selected to simulate the action process of this warhead. Explosive and air adopt the Euler algorithm. Fragments, endplates, liner and shell adopt the Lagrange algorithm. The interaction between them is simulated by the coupled Eulerian-Lagrangian (CEL). Comp. B is modeled by the material model of HIGH EXPLOSIVE BURN and the equation of JWL. The air adopts NULL material and LINEAR POLYNOMIAL equation of state. The shell and endplates are #45 STEEL and can be described by the material model of PLASTIC KINEMATIC. The liner is 2A12 and can be characterized as the material model of PLASTIC KINEMATIC. Research has shown that when the liner exists, the deformation of the fragments is very small [20]. Therefore, tungsten fragments are considered as rigid. Table 1 lists the parameters of materials [12, 13]. When the calculation time reaches 200 μs, the velocity of fragments has stabilized. The motion information of prefabricated fragments is extracted.

Table 1. Parameters of materials

Material	Parameter							
Comp. B	ρ [g/cm^3]	D [m/s]	P [GPa]	A [GPa]	B [GPa]	R_1	R_2	ω
	1.717	7980	29.5	542.23	7.678	4.2	1.1	0.34
Air	ρ [g/cm^3]	C_1	C_2	C_3	C_4	C_5	C_6	
	0.00129	0	0	0	0.4	0.4	0	
2A12	ρ [g/cm^3]	E [GPa]	μ	σ_s [GPa]	β'			
	2.7	72	0.33	0.31	0.7			
#45 STEEL	ρ [g/cm^3]	E [GPa]	μ	σ_s [GPa]	β'			
	7.83	210	0.30	0.352	0.3			
93W	ρ [g/cm^3]	E [GPa]	μ					
	17.51	117	0.22					

2.2.2 Model validation

In Zhang's study, the static explosion experiment of a prefabricated fragment warhead was carried out [17]. The fragment velocity at a certain distance in the aimable direction was measured by a laser screen. And then, the initial velocity of the fragment was obtained by solving the fragment exterior ballistic equation shown in Equation 4. The velocity attenuation coefficient a is 0.043723.

$$\begin{cases} v = \sqrt{\left(\dfrac{dx}{dt}\right)^2 + \left(\dfrac{dy}{dt}\right)^2 + \left(\dfrac{dz}{dt}\right)^2} \\ \dfrac{d^2x}{dt^2} = -av\dfrac{dx}{dt} \\ \dfrac{d^2y}{dt^2} = -av\dfrac{dy}{dt} \\ \dfrac{d^2z}{dt^2} = -av\dfrac{dz}{dt} - g \end{cases} \tag{4}$$

To verify the rationality of our finite element model, the explosion process of Zhang's warhead is simulated. The simulation and experiment of fragment velocity are compared in Table 2. Due to the limited size of the laser screen,

the fragment with the highest velocity may not pass through the screen. The fragments passing through the screen can be selected by solving the Equation 4. The maximum error e_{vmax} between the simulation and experiment of the maximum initial velocity $v_{c,max}$ of the fragments passing through the screen is 5.5%. Table 2 also lists the average initial velocity $v_{c,mean}$ for a comprehensive comparison. The maximum error $e_{c,mean}$ is –2.7%, which is acceptable to verify our numerical model. The finite element model is reasonable and can be used to analyze subsequent problems.

Table 2. Comparison of the initial velocity of fragments

Initiation scheme	Type of result	$v_{c,max}$ [m/s]	e_{vmax} [%]	$v_{c,mean}$ [m/s]	e_{vmean} [%]
Single point on the center of the end face	experiment	2026.3	2.1	2006.7	–2.5
	simulation	2069.8		1957.5	
Sequential initiation of eccentric 2 lines	experiment	2437.7	5.5	2370.4	–1.7
	simulation	2571.0		2330.3	
Sequential initiation of eccentric 3 lines	experiment	2427.6	3.6	2367.9	–2.7
	simulation	2515.3		2304.9	

3 Asynchronous Initiation between Lines

3.1 Influence of delay on orientation characteristics

Generally, the more the number of initiation lines on the circumference of the warhead, the higher precision of the directional strike. However, four to eight initiation lines are generally evenly arranged due to the limitations of warhead size, process complexity and cost [2, 4]. Figure 4 shows the frequently-used sextile initiation. When the Nos. 1 and 2 lines initiate simultaneously, the orientation direction is the positive direction of the *x*-axis. When the No. 6 and Nos. 1-3 lines initiate simultaneously, the orientation direction is also the positive direction of the *x*-axis. When the Nos. 1-3 lines initiate simultaneously, the included angle between the orientation direction and the positive direction of the *x*-axis is 30°. When No. 2 line initiates individually or Nos. 1 and 3 lines initiate simultaneously, the included angle is also 30°. Therefore, the orientation accuracy of traditional sextile initiation is 30°.

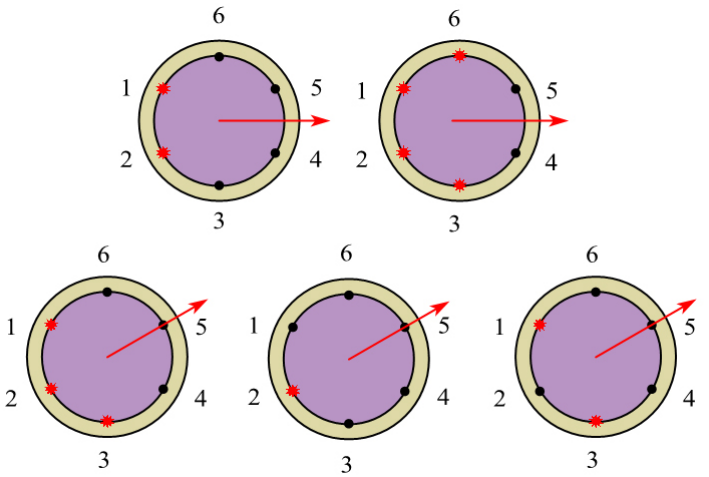

Figure 4. Orientation accuracy under sextile initiation

3.1.1 Trajectory under eccentric two-line initiation

Asynchronous initiation can deflect the trajectory of the high-pressure area and affect its action position. Regardless of the rotatable warhead, this section further refines the orientation angle through asynchronous initiation between lines without adding the initiation quantile. If the No. 2 line initiates before No. 1 in Figure 4, the trajectory equation of the high-pressure area moving to the right is as follows.

$$\begin{cases} x = \dfrac{-\sqrt{3}R^3 + \sqrt{R^2\left(R^2 - D^2\Delta t^2\right)\left(D^2\left(\Delta t + 2t\right)^2 - R^2\right)}}{2R^2} \\ y = \dfrac{D^2\Delta t\left(\Delta t + 2t\right)}{2R} \end{cases} \tag{5}$$

The azimuth of the action of high-pressure area is φ, which is the included angle between the positive x-axis and the connecting line of the high-pressure action position and the circle center. The counterclockwise direction is positive. The φ should be consistent with the miss direction θ of the target to strike directionally by adjusting the delay. When the φ are 15°, 30° and 45°, the delay are 1.109, 2.199 and 3.252 μs, respectively. The trajectories of the corresponding high-pressure area are shown in Figure 5. Under the two-line simultaneous

initiation, the high-pressure area moves along a straight line. Under asynchronous initiation, the trajectories of the high-pressure area deviate to the delayed initiation line. The offset distance is y in Equation 5. It increases with the increase of delay, detonation velocity and time, and decreases with the increase of warhead radius.

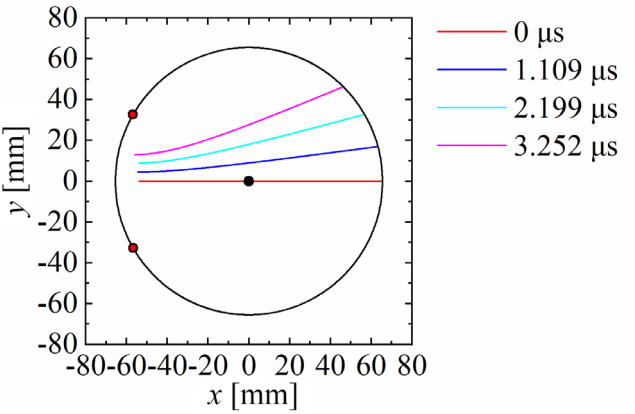

Figure 5. Trajectory of high-pressure area under eccentric two-line initiation

3.1.2 Circumferential distribution of fragment velocity

Four initiation points are set at equal intervals in each initiation line, and they detonate simultaneously [11]. Figure 6 shows the circumferential distribution of fragment velocity under asynchronous eccentric two-line initiation with different delays. The arrow indicates the φ or θ. According to the characteristics of the high-pressure area [6], the orientation range marked with dotted lines is 30° whose bisector is the orientation direction. Compared with fragments in other ranges, the velocity gain in the directional area mainly comes from fragments with the velocity higher than 2200 m/s. Therefore, fragments with the speed higher than 2200 m/s could be regarded as high-speed fragments in this warhead, and their number is recorded as N_{2200}. With the increase of time delay, the position of high-speed fragments moves counterclockwise with the high-pressure area, and the high-speed fragments become fewer and more dispersed.

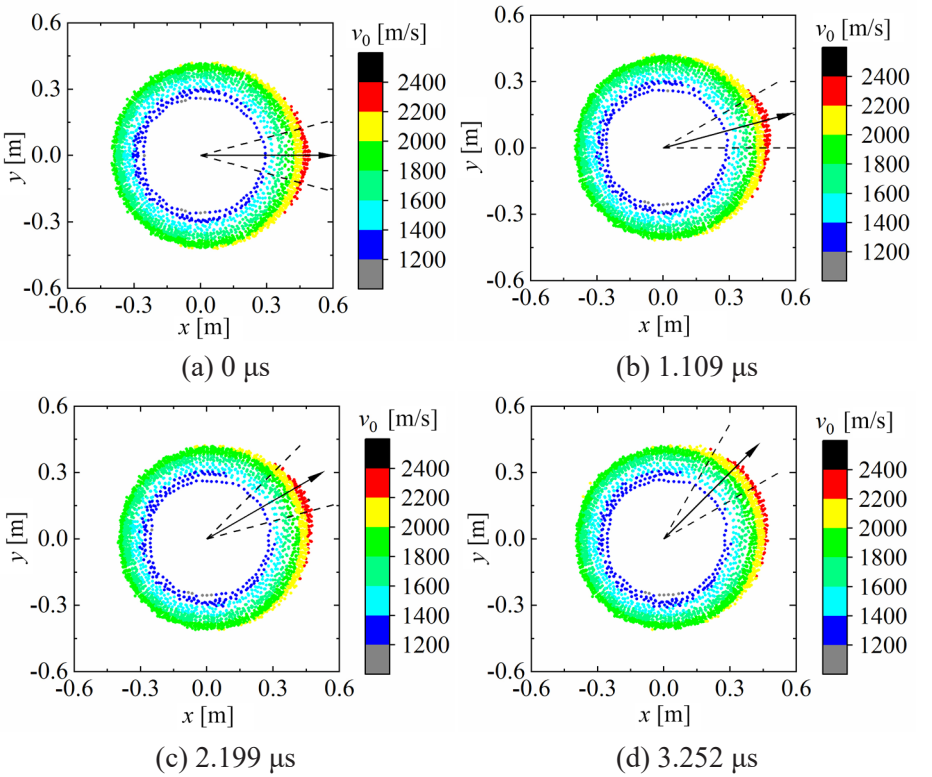

Figure 6. Circumferential distribution of fragment velocity under eccentric two-line initiation

Taking 30° as the interval angle, Figure 7 shows the average velocity v_{mean} of fragments under different delays in each interval. It can be seen that v_{mean} does not change significantly with the circumferential azimuth when a single initiation point is in the center of the warhead end face. Under eccentric initiation, the v_{mean} on the directional side is bigger than that under single point initiation, the v_{mean} on the initiation side is smaller than that under single point initiation, and the v_{mean} in the lateral side is close to that under single point initiation. The maximum value of v_{mean} under eccentric initiation is located in the high-pressure area except for 3.252 μs. The number of high-speed fragments in the directional area is also small. Therefore, the v_{mean} in the directional area is slightly smaller than that in the adjacent area under that delay. With the delay increasing, the v_{mean} in the directional area decreases, but the difference is less than 100 m/s.

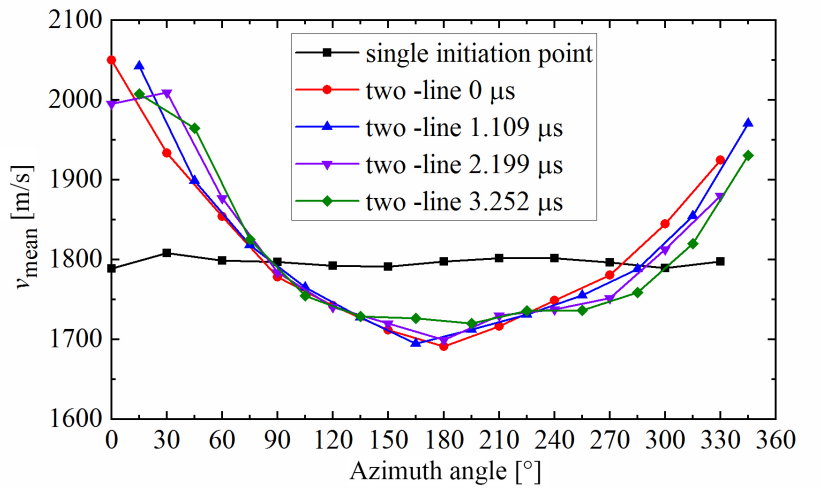

Figure 7. Circumferential distribution of v_{mean}

Compared with the single point initiation, the gain G_{vmean} of v_{mean} in the directional area is 14.6%, 13.6%, 11.1%, and 9.1% when the delay is 0, 1.109, 2.199 and 3.252 μs, respectively. The fragments with the biggest velocity are located in their directional area. Compared with the single point initiation, the gain G_{vmax} of v_{max} in the directional interval is 19.0%, 19.7%, 21.0%, and 20.2%, respectively.

3.1.3 Orientation characteristics under eccentric two-line initiation

Figure 8 shows the position (x_i, y_i) and velocity (vx_i, vy_i) of the No. i fragment in the directional area. Circumferential azimuth δ_i describes the fragment's location. Circumferential dispersion direction angle ε_i describes the fragment's scattering direction. The δ_i and ε_i of high-speed fragment in the directional area are shown in Equation 6.

$$\begin{cases} \delta_i = \arctan\dfrac{y_i}{x_i} \\ \varepsilon_i = \arctan\dfrac{v_{yi}}{v_{xi}} \end{cases} \tag{6}$$

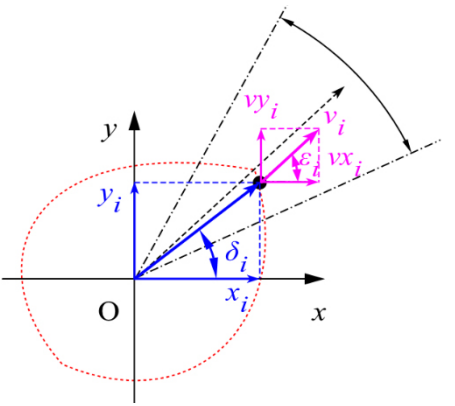

Figure 8. Position and velocity of the No. *i* fragment

High-speed fragments should be located at the target miss direction and fly in this direction to strike directionally. The azimuth δ of the high-speed fragments group is defined as the mean value of the δ_i. The circumferential dispersion direction angle ε of the high-speed fragments group is defined as the mean value of the ε_i. Table 3 shows the orientation characteristics of high-speed fragments in the directional area. It can be seen that the δ and ε increase with θ. The high-speed fragments are close to the high-pressure area and fly towards the direction of the target. The smaller the delay, the more accurate the directional control. When the target is at an azimuth of 45°, the orientation deviation is large when using the Nos. 1 and 2 initiation lines. However, asynchronous initiation with Nos. 2 and 3 initiation lines should achieve more accurate orientation. Therefore, the initiation strategy at an angle of 45° should be similar at 15°.

Table 3. Orientation characteristics of fragments

θ [°]	0.0	15.0	30.0	45.0
δ [°]	0.0	13.6	25.6	39.7
ε [°]	–0.1	13.6	25.7	39.5

No. 2 initiation line initiates before No. 1 line. The radius of the detonation wave generated by the former is larger. The detonation wave collision under the asynchronous initiation between lines is asymmetric. The high-pressure area moves towards the later initiation line. The high-pressure area is weaker than the high-pressure area produced by the symmetrical collision. Therefore, the fragment power characteristics in the directional area weaken with the increase of time delay. In addition to the high-pressure area, C-J detonation wave also

has an apparent driving effect on fragments. In particular, the detonation wave initiated first has a strong driving effect on fragments after propagating through a long path. Thus, high-speed fragments are asymmetric and biased to the first initiation line in Figure 6, which causes the orientation accuracy to deteriorate with the increase of delay.

The asynchronous eccentric two-line initiation between lines can control orientation and improve power. By selecting two adjacent lines and setting an appropriate delay between lines, the target in any direction can be damaged.

3.2 Influence of delay on power characteristics

3.2.1 Trajectory under eccentric three-line initiation

Under the eccentric three-line simultaneous initiation, two high-pressure areas generated by the collision of adjacent detonation waves collide and converge at the center of the charge and then act on the fragment after linear propagation. Compared with the eccentric two-line simultaneous initiation, the fragment velocity under this initiation mode has no apparent gain, and the number of high-speed fragments is small. The time of collision can be controlled by changing the trajectory of the high-pressure area, so it is expected to regulate the power characteristics. The eccentric three-line asynchronous initiation in which the middle line initiates first, and then two lines on both sides initiate at the same time after delay is adopted in this section. The effect of initiation delay on power characteristics is studied to improve the power.

For research convenience, the warhead in Figure 4 is rotated clockwise around the center of the circle by 30°. The middle initiation line is located on the negative of the x-axis. By substituting "$\alpha = 180°$, $\beta = 120°$" into Equation 1, the trajectory of the high-pressure area above the x-axis before convergence is expressed as follows.

$$\begin{cases} x = \dfrac{\sqrt{3}\sqrt{R^2\left(R^2 - D^2\Delta t^2\right)\left(D^2\left(\Delta t + 2t\right)^2 - R^2\right)} + D^2 R\Delta t\left(\Delta t + 2t\right) - 3R^3}{4R^2} \\ y = \dfrac{-\sqrt{3}\sqrt{R^2\left(R^2 - D^2\Delta t^2\right)\left(D^2\left(\Delta t + 2t\right)^2 - R^2\right)} + 3D^2 R\Delta t\left(\Delta t + 2t\right) + 3R^3}{4\sqrt{3}R^2} \end{cases} \tag{7}$$

According to Equation 7, the delays are 1.454 and 2.199 μs when the convergence point is at (R/2, 0) and (R, 0). When the high-pressure area output

at azimuth angles of ±15°, ±30° and ±45° dispersedly, the delays are 3.252, 4.249 and 5.173 μs, respectively. Figure 9 shows the trajectories of the high-pressure area under different delays. The convergence of the high-pressure area is delayed with increasing delay. The convergence point moves to the right along the *x*-axis. When the time delay is large, the high-pressure areas move dispersedly instead of converging. The interval of the output position increases with the increase of delay.

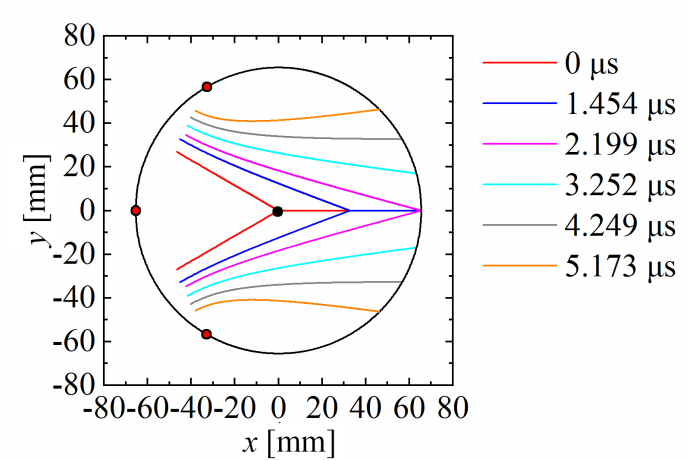

Figure 9. Trajectory of the high-pressure area under eccentric three-lines initiation

3.2.2 Power characteristics under eccentric three-line initiation

Figure 10 shows the circumferential distribution of initial velocity under different delays and marks the range of orientation area. It can be seen that eccentric three-line initiation can improve the initial velocity of fragments in the orientation area. When the time delay is small, the high-pressure areas converge and act on the fragments. The velocity of fragments is high, and the high-speed fragments concentrate in the directional area. The directional strike is powerful, which can strike the long-distance target directionally. When the delay is large, the high-speed fragments are dispersed. The strike range is large, which can cause large-area damage to the short-distance target. When the delay is 4.249 μs, the fragment with the biggest velocity is no longer located in the directional area.

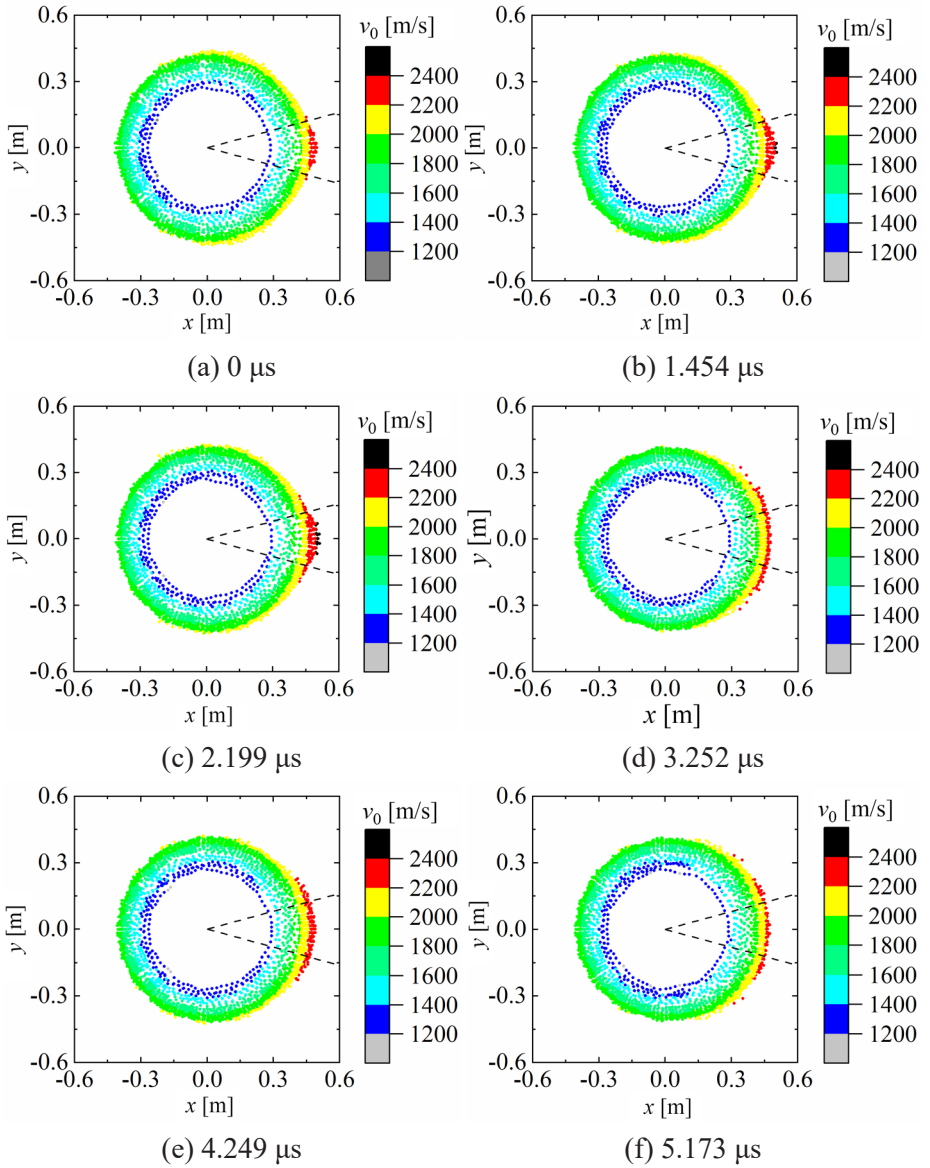

Figure 10. Circumferential distribution of fragment velocity under eccentric three-line initiation

Due to their flexibility and antagonism, air targets should be damaged by high-speed fragments [1]. The information of fragments moving to a distance

of 15 m is obtained by solving Equation 4. The attenuation coefficient a of the spherical tungsten alloy fragment with a diameter of 6 mm is 0.035411 [12]. The kinetic energy of fragments that can break through metal aircraft is 981-1962 J [21]. Fragments with kinetic energy higher than the median value of 1471.5 J are regarded as effective fragments. The number of effective fragments is recorded as N_e. Table 4 lists the power characteristics of fragments in the orientation area under eccentric three-line initiation. Four power parameters increase first and then decrease with the increase of delay. When the delay is 2.199 μs, the initial velocity of fragments is the largest, and the number of high-speed fragments and the number of effective fragments are both the largest. Compared with the single point initiation, eccentric two-line simultaneous initiation and eccentric three-line simultaneous initiation, the gain of v_{max} is 23.6%, 3.9%, 4.3%, and the gain of v_{mean} is 17.2%, 2.3%, 3.3%, respectively. Compared with eccentric three-line simultaneous initiation, the number of high-speed fragments increased by 68.8%, and the number of effective fragments increased by 23.3%. When the delay is 2.199 μs, the high-pressure areas collide and converge near the fragments. The pressure acting on fragments is high, so the initial velocity of the fragments is high. Therefore, 2.199 μs can be set as the time delay between lines to improve the power characteristics in this warhead.

Table 4. Power parameters under eccentric three-line initiation

Δt [μs]	v_{max} [m/s]	v_{mean} [m/s]	N_{2200}	N_e
0	2374	2030	80	180
1.454	2449	2073	122	205
2.199	2476	2097	135	226
3.252	2377	2056	104	222
4.249	2315	2014	68	184
5.173	2316	1997	48	174

The power gain can be realized by eccentric three-line asynchronous initiation. When the target is located in the direction of one initiation line, eccentric three-line asynchronous initiation should be adopted. The delay should cause the high-pressure area to collide just on the contact surface between charge and fragments. According to Equation 7, the expressions of delay Δt and convergence time t_c are as follows.

$$\begin{cases} \Delta t = \dfrac{\left(2-\sqrt{3}\right)R}{D} \\ t_c = \dfrac{\sqrt{3}R}{D} \end{cases} \tag{8}$$

3.3 Asynchronous initiation strategy

The best initiation strategy will be obtained by comparing the power characteristics and directional characteristics of different initiation schemes. Table 5 lists the initiation schemes that can be taken when the target is located in different miss directions in Figure 11. The interval of θ is 15°, t_i is the initiation time of the No. i initiation line. The fragment information between the –15° and 15° under single point initiation is also given. Under this initiation mode, the fragment has low power and no directional ability.

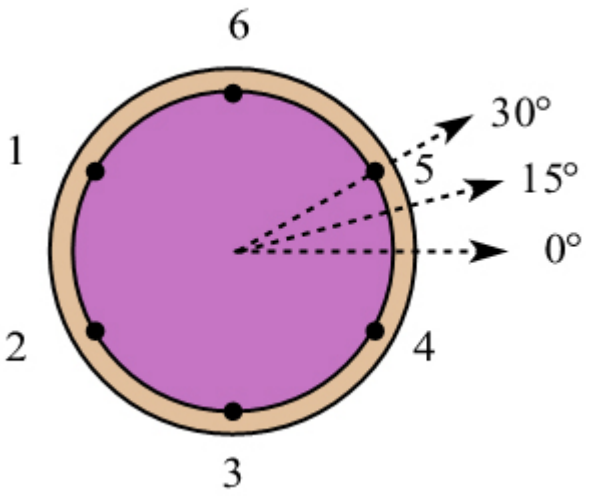

Figure 11. Diagram of different miss directions

Table 5. Sextile initiation schemes under different target orientations

θ [°]	Initiation scheme		Power characteristics				Directional characteristics		Preferred strategy
	Line	Time	v_{max} [m/s]	v_{mean} [m/s]	N_{2200}	N_e	δ [°]	ε [°]	
0-360	single point on the center of the end face		2003	1789	0	0	–	–	–
0	1, 2	$t_1 = t_2$	2383	2050	97	211	0.0	0.1	
	3, 6	$t_3 = t_6$	2202	1819	2	13	0.0	0.0	
	6, 1, 2, 3	$t_1 = t_2 = t_3 = t_6$	2352	1896	2	79	–0.1	–0.1	
	6, 1, 2, 3	$t_1 = t_2$ $t_3 = t_6$; $t_6 - t_1 = 4.249$ μs	2514	2114	135	214	0.0	0.0	√
15	1, 2	$t_1 - t_2 = 1.109$ μs	2392	2042	93	195	13.6	13.6	√
	1, 2	$t_1 = t_2$[a)]	2368	2018	64	187	10.0	10.1	
	1, 2, 3	$t_1 = t_2 = t_3$[a)]	2364	1972	43	150	21.6	21.6	
30	2		2320	1966	26	143	27.5	27.6	
	1, 3	$t_1 = t_3$	2379	1969	51	145	29.8	29.9	
	1, 2, 3	$t_1 = t_2 = t_3$	2418	2009	77	166	28.9	29.0	
	1, 2	$t_1 - t_2 = 2.199$ μs	2407	2009	70	183	25.6	25.7	
	1, 2, 3	$t_3 - t_2 = 2.199$ μs $t_1 - t_2 = 2.199$ μs	2582	2077	115	211	30.3	30.4	√

[a)] The scheme that can be adopted to strike the target in this direction when the asynchronous initiation between lines is not adopted

When the target miss azimuth θ is 0°, two or four symmetrical initiation lines can be selected. Under simultaneous initiation, the power and directional ability of adjacent eccentric two-line initiation are optimal. More lines do not mean better performance, because the detonation waves converge and offset at the center of the warhead. Under the asynchronous four-line initiation, the No. 1 and No. 2 initiation lines detonate first, and the No. 3 and No. 6 initiation lines detonate later can also achieve strike. The delay required for the convergence of the three high-pressure zones at (0, R) is 4.249 μs. Eccentric four-line asynchronous initiation should be used because of its high power and accurate orientation. Asynchronous initiation can adjust the movement direction of the high-pressure area and make them finally converge to drive fragments together. When the θ is 15°, eccentric two-line or three-line simultaneous initiation can be used before the asynchronous initiation scheme between lines is adopted. However, due to the deviation between the high-pressure area and target orientation, the power and accuracy of fragments in the orientation area are insufficient. Thus, asynchronous initiation should also be adopted. Asynchronous initiation can

make the high-pressure area act on the target orientation. The fragment velocity in the directional area increase, and the fragments fly to the target. When the θ is 30°, one or more symmetrical initiation lines can be selected. Among the original initiation schemes, the eccentric three-line simultaneous initiation has the strongest power. When the asynchronous detonation scheme is adopted, the power of the fragment is enhanced. Eccentric three-line asynchronous initiation is preferred because of power and accuracy.

The initiation strategy for targets in different directions is shown in Figure 12. Compared with the single point initiation, the gain of maximum velocity under this optimal strategy is 19.7-29.8%, and the gain of average velocity is 13.6-18.2%. When the target is outside 0-30°, the preferred initiation strategy is similar to Table 5 and Figure 12 in addition to selecting different initiation lines.

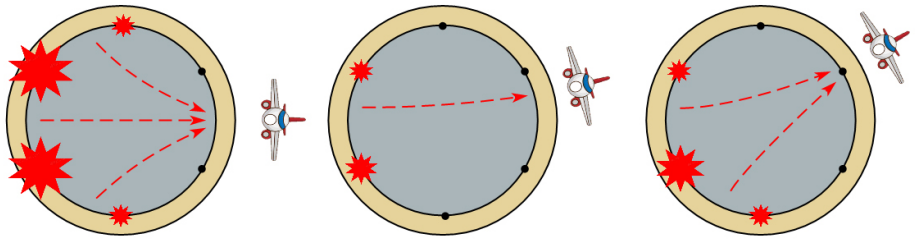

(a) 0° (b) 15° (c) 30°

Figure 12. Initiation strategies for targets in different directions

The orientation accuracy of simultaneous initiation under twelve quantiles is 15°, which is shown in Figure 13. Many simultaneous initiation schemes can be used to attack the target at the same azimuth. Table 6 compares them under different target azimuth angles, where t_i is the initiation time of the No. i initiation line in Figure 13. The same schemes as the sextile initiation are not listed repeatedly.

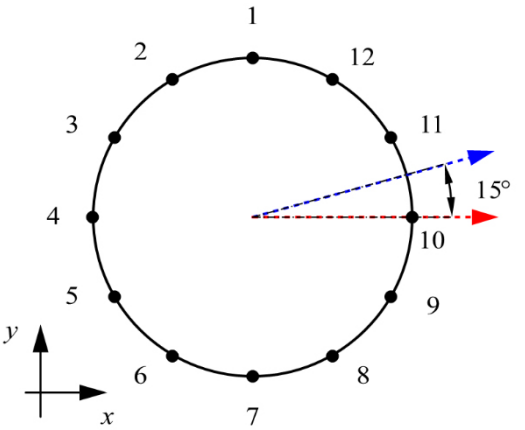

Figure 13. Diagram of 12 quantiles initiation

Due to the symmetrical initiation lines, the orientation accuracy of these schemes is enough. Therefore, the power characteristic is our attention. As shown in Table 6, the best scheme is to initiate several adjacent lines instead of alternating lines, which is the result of the trade-off between pressure and pressure distance [3]. Initiate the adjacent lines on the opposite side of the target, and shall not include the detonating line close to the normal direction. Because the high-pressure area under multi-lines initiation will converge at the center, their opposite driving effect will be offset.

The effect of asynchronous initiation can be illustrated by comparing Tables 5 and 6. When the θ is 0°, the power characteristics of the best initiation scheme in Table 5 are better than those in Table 6. When the θ is 15°, the best scheme in Table 5 is slightly inferior to that in Table 6, but better than other schemes in Table 6. The best scheme in Table 5 when the θ is 30° is better than the best scheme in Table 6 when the θ is 0°. Therefore, the results of sextile asynchronous initiation are similar to or even better than that of simultaneous initiation under twelve quantiles. Considering that it is more challenging to realize the twelve quantiles initiation in a small-caliber warhead, sextile asynchronous initiation is a better choice.

Table 6. Simultaneous initiation schemes under twelve quantiles

θ [°]	Initiation lines	Power characteristics				Directional characteristics		Preferred strategy
		v_{max} [m/s]	v_{mean} [m/s]	N_{2200}	N_e	δ [°]	ε [°]	
0	3, 4, 5	2391	2064	108	219	0.0	0.0	√
	2, 6	2344	1990	42	157	–0.1	–0.1	
	2, 3, 4, 5, 6	2397	2052	104	201	0.1	0.1	
	1, 2, 3, 4, 5, 6, 7	2360	1924	8	106	0.3	0.3	
	1, 2, 4, 6, 7	2343	1903	2	86	0.0	0.0	
	1, 3, 4, 5, 7	2359	1904	2	87	0.0	0.0	
15	4, 5	2380	2028	75	191	15.9	16.0	
	3, 6	2463	2036	83	182	15.4	15.5	
	2, 7	2260	1890	6	71	16.5	16.7	
	3, 4, 5, 6	2529	2075	112	203	15.2	15.3	√
	2, 3, 4, 5, 6, 7	2389	1977	43	150	15.8	16.0	
	2, 4, 5, 7	2369	1956	33	133	15.7	15.8	
	2, 3, 6, 7	2354	1946	24	125	14.8	15.0	

To verify the practicability of the asynchronous initiation between lines, a warhead with a diameter of 300 mm is studied. In Table 7, the results of sextile asynchronous initiation and twelve quantiles simultaneous initiation are compared. Due to the increase of charging ratio, the velocity of fragments is higher than that of warheads with a diameter of 155 mm. After comparison, the fragment with speed higher than 2700 m/s could be regarded as high-speed in this warhead. The number of high-speed fragments N_{2700} and corresponding δ, ε are also listed in Table 7. When the θ is 0° or 30°, sextile asynchronous initiation is better. While simultaneous initiation under twelve quantiles is better when the θ is 15°. Thus, asynchronous initiation between lines still has certain advantages in large-caliber warheads.

Table 7. Sextile asynchronous initiation and twelve quantiles simultaneous initiation in large-caliber warhead

θ [°]	Initiation scheme		Power characteristics				Directional characteristics		Better
	Quantile	Time	v_{max} [m/s]	v_{mean} [m/s]	N_{2700}	N_e	δ [°]	ε [°]	
0	12	$t_3 = t_4 = t_5$	3167	2488	203	613	0.1	0.2	
	6	$t_1 = t_2$ $t_3 = t_6$ $t_6 - t_1 = 8.925$ μs	3512	2579	241	609	0.2	0.2	√
15	12	$t_3 = t_4 = t_5 = t_6$	3306	2504	211	616	14.9	15.0	√
	6	$t_1 - t_2 = 2.337$ μs	3099	2431	152	599	12.6	12.5	
30	12	$t_4 = t_5 = t_6$	3212	2458	184	633	29.8	29.9	
	6	$t_4 - t_5 = 4.634$ μs $t_4 = t_6$	3449	2520	230	644	29.5	29.6	√

The process of asynchronous initiation strategy between lines under sextile initiation is shown in Figure 14. Two to four initiation lines on the opposite side of target should be selected according to the miss direction. The initiation delay is calculated according to the diameter of charge, the detonation velocity of charge and the setting of initiation lines. When the target is located on the bisector of the included angle of the initiation lines, the eccentric four-line asynchronous initiation should be adopted, and the initiation delay should make the high-pressure area converge at the fragments. When the target is in the direction of one initiation line, the eccentric three-line asynchronous initiation should be adopted, and the delay should also make the high-pressure area converge at the fragments. Otherwise, eccentric two-line asynchronous initiation shall be adopted, and the initiation delay shall make the high-pressure area act on the target direction.

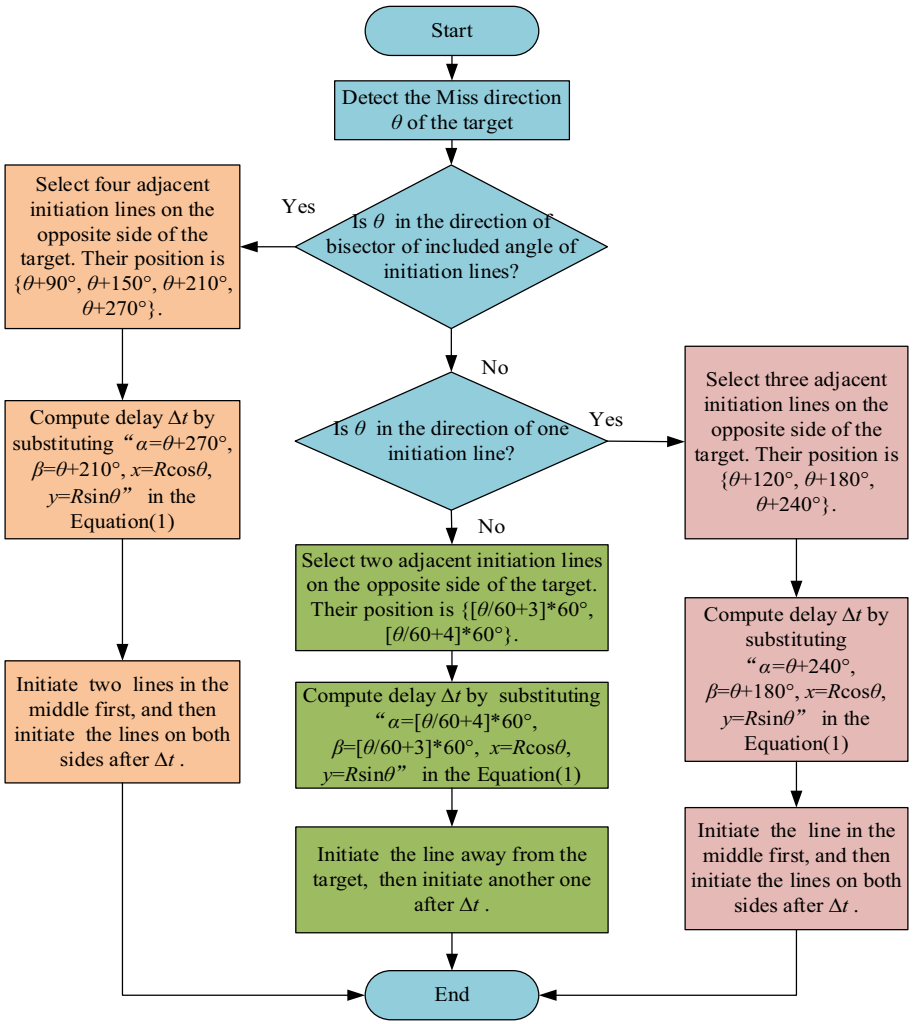

Figure 14. Flow chart of initiation strategy algorithm

3.4 Initiation strategy with single delay

If only one initiation delay can be adopted, the directional accuracy can be doubled using asynchronous initiation between lines. When the initiation quantile is n, the delay between lines can be solved by substituting "$x=R\cos(\pi/(2n))$, $y=R\sin(\pi/(2n))$" into Equation 5. This delay can improve the accuracy from π/n to $\pi/(2n)$. Under sextile initiation, the delay is shown in Equation 9. The delay of the warhead with a diameter of 155 mm should be set to 1.109 μs to achieve the angle resolution of 15°under sextile initiation.

$$\Delta t = \sqrt{4 + \frac{3\sqrt{2}}{2} + \frac{\sqrt{6}}{2} - 2\sqrt{5 + 3\sqrt{2} + \sqrt{3} + \sqrt{6}}}\,\frac{R}{D} \approx 0.13513\frac{R}{D} \tag{9}$$

Table 8 lists two new schemes under the single delay. When the angle the θ is 0°, the initiation strategy in Table 8 is worse than eccentric two-line simultaneous initiation in Table 5. When the θ is 30°, the power of the scheme in Table 8 is slightly worse than the delay of 2.199 μs but better than the other four initiation schemes in Table 5. Asynchronous initiation can improve the effect of simultaneous initiation. However, the improvement effect of the single delay is limited.

Table 8. New initiation schemes of the single delay

θ [°]	Lines	Time	v_{max} [m/s]	v_{mean} [m/s]	N_{2200}	N_e	δ [°]	ε [°]
0	6, 1, 2, 3	$t_1 = t_2$, $t_3 = t_6$ $t_6 - t_1 = 1.109$ μs	2330	1929	9	117	0.0	0.0
30	1, 2, 3	$t_1 = t_3$ $t_1 - t_2 = 1.109$ μs	2492	2039	98	183	29.7	29.8

Table 9 shows the optimal strategy based on the asynchronous initiation between lines when the target is located in different miss directions. Compared with the single point initiation, the gain of the maximum initial velocity of fragments is 19.0-25.3%, and the gain of the average initial velocity is 12.8-14.6%. The maximum deviation of fragment orientation azimuth and flight direction are both –1.4°.

Table 9. Initiation strategy with single delay

θ [°]	Initiation mode		G_{vmax} [%]	G_{vmean} [%]	e_δ [°]	e_ε [°]
	Lines	Time				
0	1, 2	$t_1 = t_2$	19.0	14.6	0.0	0.1
15	1, 2	$t_1 - t_2 = 1.109$ μs	19.7	13.6	–1.4	–1.4
30	1, 2, 3	$t_3 - t_2 = 1.109$ μs $t_1 - t_2 = 1.109$ μs	25.3	12.8	0.3	0.2

Each initiation quantile should be independent and has at least three output modes: normal output, delayed output, and no output. It can be realized by the slapper detonator or explosive logic circuit. Simultaneous initiation in the same initiation line can be realized through simultaneous linear initiation network.

4 Conclusions

The following conclusions are drawn from this study:

- The target in any direction can be struck by selecting the initiation lines on the opposite side of target and setting an appropriate delay. Under eccentric two-line initiation, with the increase of delay between lines, the trajectory offset of the high-pressure area increases, the average velocity of fragments in the directional region decreases, the number of high-speed fragments decreases, the azimuth of high-speed fragments increases, and the deviation of directional angle increases.
- Setting an appropriate delay between lines can improve the power of fragments in the directional area. Under eccentric three-line initiation, there is delayed convergence or even no convergence of the high-pressure area with the increase of delay. The power characteristics of fragments increase and then decrease with the increase of delay. The fragment velocity is the highest when the convergence position of the high-pressure areas is located on the contact surface between charge and fragments. Compared with the single point initiation and eccentric three-line simultaneous initiation, the gain of maximum velocity is 23.6% and 4.3%, respectively.
- Asynchronous initiation between lines can improve the accuracy and power without increasing the initiation quantile. The preferred strategies under sextile asynchronous initiation are similar to or even better than that of simultaneous initiation under twelve quantiles. Especially, the accuracy can be improved from 30° to 15° by setting a single delay of 1.109 μs under sextile initiation. Compared with the single point initiation, the gain of the maximum initial velocity of fragments is 19.0-25.3% under this initiation strategy. The maximum deviation of fragment orientation azimuth and flight direction are both –1.4°.

Acknowledgements

This work was supported by the National Natural Science Foundation of China and the China Academy of Engineering Physics under Grant No. U15301135.

References

[1] Waggener, S. The Evolution of Air Target Warheads. *Proc. 23th Int. Symp. Ballistics,* Tarragona, Spain, **2007**, pp. 67-75.

[2] Waggener, S. Relative Performance of Anti-Air Missile Warheads. *Proc. 19th Int. Symp. Ballistics*, Interlaken, Switzerland, **2001**, pp. 7-11.

[3] Li, Y.; Xiong, S.; Li, X.; Wen, Y.Q. Mechanism of Velocity Enhancement of Asymmetrically Two Lines Initiated Warhead. *Int. J. Impact Eng.* **2018**, *122*: 161-174; https://doi.org/10.1016/j.ijimpeng.2018.07.011.

[4] Held, M. Fuze Sensor Requirements of the Different Aimable Anti Air Warhead Layouts. *Proc. 23th Int. Symp. Ballistics,* Tarragona, Spain, **2007**, pp. 16-20.

[5] Xia, H.J.; Cui, Z.Z.; Zhou, R.J. *Overall Technology of Proximity Detection and Damage Control.* Beijing Institute of Technology Press, Beijing, **2019**, pp. 239-253; ISBN 9787568271899.

[6] Shen, H.M.; Li, W.B.; Wang, X.M. Velocity Distribution of Fragments Resulted by Explosion of a Cylindrical Shell Charge on multi-Spots Eccentric Initiation. (in Chinese) *Explos. Shock Waves* **2017**, *37*(6): 1039-1045.

[7] Xu, H.Y.; Li, W.B.; Li, W.B.; Zhang, Q.; Wang, Y.J.; Hong, X.W. Fracture Mechanism of a Cylindrical Shell Cut by Circumferential Detonation Collision. *Def. Technol*. **2021**, *17*: 1650-1659; https://doi.org/10.1016/j.dt.2020.09.006.

[8] Guo, Z.W.; Huang, G.Y.; Zhu, W.; Feng, S.S. The Fragmentation of D-shaped Casing Filled with Explosive under Eccentric Initiation. *Def. Technol*. **2018**, *14*: 417-421; https://doi.org/10.1016/j.dt.2018.06.006.

[9] Dhote, K.D.; Murthy, K.P.S.; Rajan, K.M.; Sucheendran, M.M. Directional Warhead Design Methodology for a Tailored Fragment Beam. *Cent. Eur. J. Energ. Mater*. **2015**, *12*(4): 637-649.

[10] Wang, S.S.; Ma, X.F.; Sui, S.Y.; Jang, Z.H. Experimental Research on Fragments Dispersion of the Warhead Under Asymmetrical Multi-Spots Initiation. (in Chinese) *Trans. Beijing Inst. Technol.* **2001**, *2*: 177-179.

[11] Li, Y.; Li, Y.H.; Liu, C.; Wen, Y.Q. The Initiation Parameter of Detonation Wave Aiming Warhead. *Chin. J. Energ. Mater.* **2016**, *24*(9): 915-921; https://doi.org/10.11943/j.issn.1006-9941.2016.09.017.

[12] Li, Y.; Wen, Y. Experiment and Numerical Modeling of Asymmetrically Initiated Hexagonal Prism Warhead. *Adv. Mech. Eng*. **2017**, *9*(1): 1-14; https://doi.org/10.1177/1687814016687966.

[13] Deng, H.; Quan, J.L.; Liang, Z.F. Influence of Eccentric Initiation on Energy Distribution Gain of Warhead Charge. (in Chinese) *Explos. Shock Waves* **2022**, *42*(5): 62-74.

[14] Earl, E. *Selectable Initiation-point Fragment Warhead.* Patent US 4658727, **1987**.

[15] Cunard, D.A.; Thomas, K.A. Programmable Integrated Ordnance Suite (PIOS). *Proc. 1st Annu. Int. Missiles and Rockets Exhibition,* **1992**.

[16] Liu, C.; Li, Y.; Li, Y.H.; Wen, Y.Q. Influence of Eccentric Initiation Ways on Fragment Dispersion Rule of Prismatic Aimable Warhead. *Chin. J. Energ. Mater.*

2017, *25*(1): 63-68.
[17] Zhang, H.Y.; Zhang, S.K.; Cheng, L.; Li, Y.; Wen, Y.Q.; Zhang, Z.W. The Impact of Initiation Mode of Blast Fragmentation Warhead on the Power to Kill the Ground Target. (in Chinese) *Acta Armamentarii* **2021**, *42*(11): 2300-2309; https://doi.org/10.3969/j.issn.1000-1093.2021.11.002.
[18] Zhang, B.P.; Zhang, Q.M.; Huang, F.L. *Detonation Physics.* Weapon Industry Press, Beijing, **2009**, pp. 189-196; ISBN 9787802483859.
[19] Zhang, S.K.; Wang, K.W.; Xie, J.L.; Li, X.G.; Zhang, H.Y.; Cheng, L. Influence of In-line Asynchronous Initiation on Warhead Damage Efficiency. (in Chinese) *Chin. J. Explos. Propellants* **2022**, *45*(01): 73-80.
[20] Li, Y.; Li, Y.H.; Wen, Y.Q. Radial Distribution of Fragment Velocity of Asymmetrically Initiated Warhead. *Int. J. Impact Eng.* **2017**, *99*: 39-47; https://doi.org/10.1016/j.ijimpeng.2016.09.007.
[21] Huang, Z.X.; Zu, X.D. *Terminal Effects.* Science Press, Beijing, **2014**, pp: 111-125; ISBN 9787030423801.

Received: October 24, 2022
Revised: March 27, 2024
First published online: March 29, 2024